Stimulated Raman scattering in Ge nanowires

Masiar Sistani, Maximilian G Bartmann, Nicholas A Güsken, Rupert F Oulton, Hamid Keshmiri, Minh Anh Luong, Eric Robin, M. den Hertog, Alois Lugstein

Stimulated Raman Scattering in Ge Nanowires

Masiar Sistani[1], Maximilian G. Bartmann[1], Nicholas A. Güsken[2], Rupert F. Oulton[2], Hamid Keshmiri[1], Minh Anh Luong[3], Eric Robin[3], Martien I. den Hertog[4], Alois Lugstein[1*]

[1] *Technische Universität Wien, Institute of Solid State Electronics, Vienna, Austria*

[2] *The Blackett Laboratory, Department of Physics, Imperial College London, London SW7 2AZ, United Kingdom*

[3] *Université Grenoble Alpes, CEA, IRIG-DEPHY, F-38054 Grenoble, France*

[4] *Université Grenoble Alpes, CNRS, Institut NEEL UPR2940, Grenoble, France*

*E-Mail Address of corresponding author: alois.lugstein@tuwien.ac.at

Investigating group-IV based photonic components is a very active area of research with extensive interest in developing complementary metal-oxide-semiconductor (CMOS) compatible light sources. However, due to the indirect band-gap of these materials, effective light emitting diodes and lasers based on pure Ge or Si cannot be realized. In this context, there is considerable interest in developing group-IV based Raman lasers. Nevertheless, the low quantum yield of stimulated Raman scattering in Si and Ge requires large device footprints and high lasing thresholds. Consequently, the fabrication of integrated, energy-efficient Raman lasers is challenging. Here, we report, a systematic investigation of stimulated Raman scattering (SRS) in Ge nanowires (NWs) and axial Al-Ge-Al NW heterostructures with Ge segments contacted to self-aligned Al leads with abrupt metal-semiconductor interfaces. Dependent on their geometry, these quasi-1D heterostructures can reassemble into Ge nanowires, Ge nanodots or Ge nanodiscs, which are monolithically integrated within monocrystalline Al (c-Al) mirrors that promote both optical confinement and effective heat-dissipation. Optical mode resonances in these nanocavities support in SRS thresholds as low as 60 kW/cm^2. Most notably, our findings provide a platform for elucidating the high potential of future monolithically integrated, nanoscale low-power group-IV based Raman lasers.

INTRODUCTION

The continuing miniaturization of Si based integrated circuits has led to high performance compact devices with reduced power consumption at lower cost.[1,2,3] Associated with this rapid downscaling, metallic interconnects have become a severe bottleneck, due to their high space demand, signal delays and electromagnetic interference.[4,5] Thus, there is an increasing demand for high-speed data transmission in the optical domain.[6] While effective on-chip detection and transmission have already been demonstrated,[7] conventional light emitting diodes and lasers based on pure Si or Ge cannot be realized, due to their indirect band-gap. In this context, there is considerable interest in developing group-IV based Raman lasers. Nevertheless, the low quantum yield of SRS in Si and Ge requires large device footprints and high lasing thresholds.[8,9] These centimeter-scale lasers are incompatible with the goal of fabricating on-chip energy efficient monolithically integrable lasers.[10,11] Meanwhile, semiconducting NWs may possess great future potential due to their quasi 1D cylindrical geometry and easy device integration.[12,13] In terms of optoelectronic devices, it was already demonstrated that NWs can function as both, active optical device elements[14] and transmission lines.[15] Lasers fabricated from direct bandgap semiconductor NWs have been achieved using GaN,[16] ZnO,[13] and CdS.[17] However, there are only a few works on NW based Raman lasers, including the pioneering work on cavity-enhanced SRS in GaP NWs[18] and cavity-mode enhanced SRS in Si NWs.[19,20] To our

knowledge, there are no further reports on this important nonlinear optical effect in semiconductor NWs.

METHODS

Device fabrication:

Vapor-liquid solid[21] (VLS) grown Ge NWs with a length of several micrometer and diameters ranging from 40 nm to 140 nm were dispersed onto a Si substrate with 100 nm of thermally grown SiO_2 atop. To synthesize the Al-Ge-Al NW heterostructures Ge NWs with diameters of 100 nm were contacted to Al pads fabricated by electron beam lithography, 150 nm Al sputter deposition, preceded by a 5s HI dip (14 %) to remove any Ge oxide, and lift-off techniques. The Al-Ge exchange reaction is induced by rapid thermal annealing (UniTemp UTP 1100) at a temperature of T = 624 K in forming gas atmosphere and results in quasi-1D NW heterostructures. To achieve small Ge nanostructure devices, such as nanodots and nanodiscs, consecutive thermal annealing steps were applied, accompanied by SEM imaging.[22,23]

Raman measurements:

A confocal μ-Raman setup (Alpha300, WITec) was employed in backscattering geometry with a grating monochromator and a CCD camera (DV401- BV, Andor). A frequency doubled Nd:YAG laser emitting linearly polarized light at λ = 532 nm was used as excitation source. The laser light passes a beam splitter with an integrated polarizer and is focused onto the sample surface through an achromatic Nikon EPI EPlan 100x objective (NA = 0.9, WD = 0.23 mm),

enabling a diffraction limited spot size of ~720 nm. The scattered light was confocally collected through the objective and filtered to remove the excitation wavelength and then coupled into a fiber that guides the light to the spectrometer.

FDTD simulations:

Numerical 3D FDTD calculations were performed (based on the commercially available software Lumerical FDTD) at λ = 532 nm incident wavelength to estimate the strength of the Raman effect from the Ge TO mode. The electrical energy inside the Ge segment was calculated by integrating the simulated integrated field intensity over the entire Ge-volume $\frac{n^2}{2}\int_{V_{Ge}}\left|E_p(\boldsymbol{r})\right|^2 dV$ with $n^2 = \varepsilon_r * \mu r$ and $\mu_r = 1$, where ε_r is the relative permittivity and μ_r the relative permeability. The data is typically normalized to the peak value, hence $\frac{n^2}{2}$ cancels out within the fraction, to provide a relative local field enhancement factor. When estimating the relative strength of Raman scattering between different Ge nanostructures, the calculated data per Ge volume was corrected by the measured signal decrease due to the temperature increase in the NW segment as explained in the supporting information.

RESULTS AND DISCUSSION

In this paper, we present a systematic experimental investigation of Raman scattering in Ge nanostructures. The VLS grown Ge NWs with a length of several micrometer and diameters ranging from 40 nm to 140 nm were dispersed onto a Si substrate with 100 nm of thermally

grown SiO_2 atop. Raman spectroscopy was performed using a confocal µ-Raman setup with CW laser excitation at λ_{Pump} = 532 nm. A schematic illustration of the µ-Raman experiments on Ge NWs in backscattering geometry is shown in Figure 1a. The Stokes Raman spectra of a NW with a diameter of 100 nm for pump laser intensities between 8 kW/cm² and 200 kW/cm² are shown in Figure 1b. The Raman spectra reveal two distinct peaks assigned to the Stokes transverse optical (TO) modes of Ge-Ge vibrations (Ge TO) at about 301 cm^{-1} and the Si-Si vibrations (Si TO) of the underlying Si substrate at 520 cm^{-1}.[24,25,26] With increasing pump laser intensity both TO modes increase in intensity but only the Ge related Raman peak undergoes a slight red shift. The inset shows the red-shift of the TO phonon mode of a 2 µm long (black) Ge NW and a 100 nm long (red) Ge NW for increasing pump intensities up to 190 kW/cm². This red-shift is associated to laser induced heating. The more pronounced red-shift of the Ge TO phonon mode is consistent with the smaller thermal mass of the shorter Ge NW.[24,27]

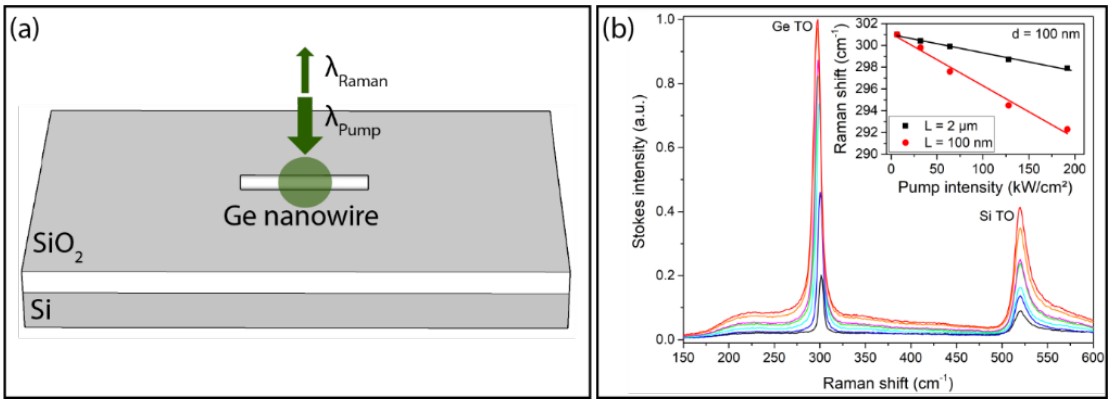

Figure 1. *(a) Schematic illustration of µ-Raman experiments on Ge NWs in backscattering geometry and confocal detection. (b) Exemplary Stokes Raman spectra of a Ge NW with a diameter of 100 nm and a length of 2 µm, for laser excitation (λ_{Pump} = 532 nm) with intensities between 8 kW/cm² and 190 kW/cm². The Raman spectrum shows the TO modes at 301 cm^{-1} and 520 cm^{-1} assigned to Ge-Ge and Si-Si vibrations of the Ge NW and the underlying Si substrate,*

respectively. The inset shows the red-shift of the Ge TO phonon mode for a 2 µm long (black) and a 100 nm long (red) Ge NW for pump intensities up to 190 kW/cm².

According to the work of Agarwal *et al.*[19,20] cavity-mode enhanced SRS in Si NWs was demonstrated to arise from higher electric field intensity and lower mode volume of the electromagnetic modes inside the quasi-1D nanostructures. To investigate the dependence of the Stokes intensity of the Ge TO peak on the Ge NW diameter, numerical calculations were performed to calculate the electric energy confined to the Ge NW *via* the finite difference time domain (FDTD) method.[19,28] The calculations shown in Figure 2a clearly reveal that for λ_{Pump} = 532 nm, the highest electric field intensity is observed for Ge NWs with a diameter of about 100 nm. The calculations were then compared with the integrated Ge TO Stokes intensity of Ge NWs with diameters between 40 nm and 140 nm. As heating not only induces red-shifts, but also decreases the Stokes intensity,[29] the recorded spectra were corrected for these temperature effects (see Figure S1). As shown in Figure 2b, Ge NWs with a diameter of 100 nm show the highest Stokes intensity. In all these cases, the Stokes intensity of the Ge TO peak increases linearly with the pump intensity, indicating spontaneous Raman scattering.[19]

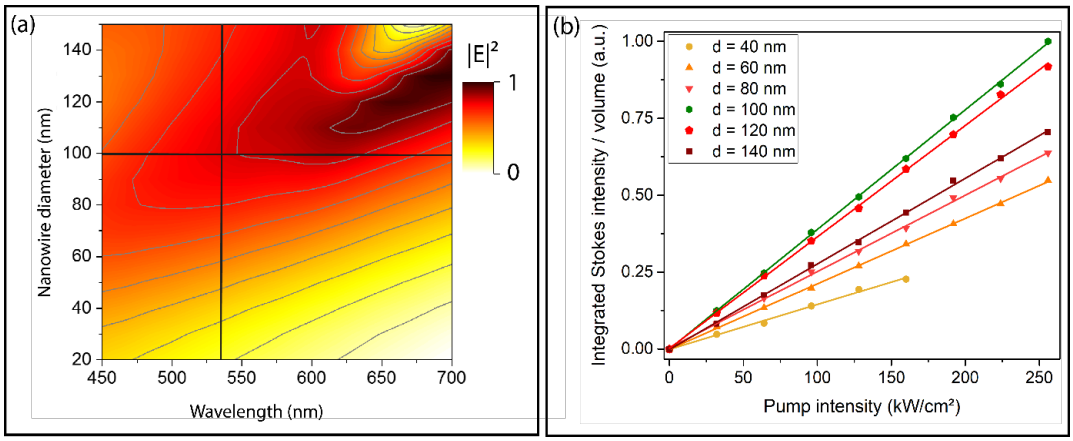

Figure 2. *(a) FDTD calculation of the spatial distribution of the electric field intensity inside Ge NWs of various diameters as a function of excitation wavelength (b) Normalized integrated*

Stokes intensity of the Ge TO peak of 2 µm long Ge NWs with different diameters at various pump intensities. The µ-Raman measurements were obtained using a λ = 532 nm pump laser and corrected with respect to thermal effects.

To cope with the problem of laser induced heating and to further achieve and explore SRS, Ge NWs were monolithically integrated in metal-semiconductor-metal (M-S-M) NW heterostructures (Figure 3a). Therefore, the Ge NWs on the oxidized Si substrate were contacted with 150 nm thick Al pads using electron beam lithography, Al sputter deposition preceded by a 5 s HI dip (14%) and lift-off techniques. To adjust the Ge NW segment length a thermally induced exchange reaction was applied using rapid thermal annealing.[22,23] This results in axial Al-Ge-Al NW heterostructures with ultra-scaled Ge segments contacted on both sides by self-aligned monocrystalline Al leads with abrupt M-S interfaces (see Figures S2 and S3). The schematics and SEM images in Figure 3b show such Al-Ge-Al NW heterostructures with typical Ge geometries further denoted as Ge segment (L > d), nanodot (L ≈ d) and nanodisc (L < d).

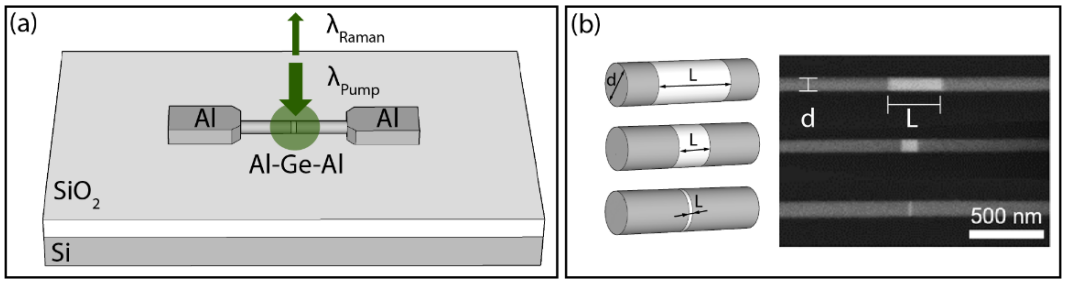

Figure 3. *(a) Schematic illustration of µ-Raman experiments on Al-Ge-Al NW heterostructures in backscattering geometry. (b) Schematic illustration and SEM images of a Ge segment (L > d), nanodot (L ≈ d) and nanodisc (L < d) monolithically integrated in an Al-Ge-Al NW heterostructure.*

The c-Al leads contacting the Ge segments are expected to effectively dissipate the energy introduced by laser excitation. Figure 4a shows the Raman shift and the corresponding calculated temperature increases at various laser pump intensities for a 100 nm long Ge NW and a Ge segment of the same length embedded in the Al-Ge-Al NW heterostructure (dashed and solid red lines, respectively). As expected, the bare Ge NW heats up significantly more than the Al-Ge-Al NW heterostructure device. This is attributed to an efficient heat transfer by the c-Al contact leads and dissipation by the large Al heat sinks. This is further supported by the investigation of various heterostructure devices between L = 500 nm and 20 nm, which revealed significantly lower laser induced heating effects for ever smaller Ge segments.

Figure 4b compares the normalized angle-dependent integrated Ge TO Stokes intensities of a Ge segment, a nanodot and a nanodisc all integrated within Al-Ge-Al NW heterostructures. Here, the electric field polarization is being rotated from being parallel (transverse magnetic, TM) to being perpendicular (transverse electric, TE) to the NW axis. Elongated Ge NWs (black) exhibit the highest integrated Stokes intensity of the Ge TO peak when the incident polarization is parallel to the NW axis. The anisotropic Raman scattering can be explained by considering the effect of the dielectric permittivity mismatch of the NW geometry.[30,31] In contrast, the Ge nanodisc (blue) shows much less anisotropy and the Stokes intensity of the Ge TO peak was found to be larger for the pump laser polarized perpendicular to the NW axis i.e. parallel to the elongated Ge nanodisc, which can again be associated to the dielectric permittivity mismatch of the geometry. However, according to the particular geometry of the nanodisc devices this effect was found to be quite weak. Finally, the Ge nanodot (red) shows no preferential polarization axis. Based on these investigations, the Raman response of the respective devices was maximized for the following investigations choosing the proper laser polarization.

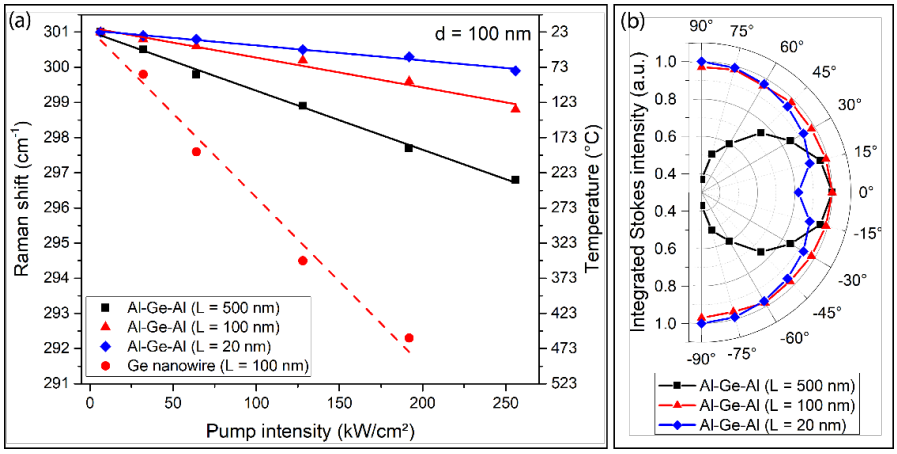

Figure 4. *(a) Comparison of the laser heating effect on the Raman shift of Ge NWs and Al-Ge-Al NW heterostructures all with a diameter of 100 nm. (b) Polar representation of the normalized angle-dependent integrated Stokes intensities of the Ge TO peak of a Ge NW (black), a Ge nanodot (red) and a Ge nanodisc (blue). All μ-Raman measurements were obtained using a λ = 532 nm pump laser.*

Importantly, the effective heat dissipation in Al-Ge-Al NW heterostructures compared to bare Ge NW devices allows an investigation of Raman scattering for higher excitation intensities without thermally damaging these devices. Determining the integrated Stokes intensity as a function of the excitation power requires subtraction of the enhanced background observed for the Al-Ge-Al heterostructures (see Figure S4). The integrated Stokes intensity of the Ge TO peak was further normalized by Ge volume for varying Ge segment length L, as a function of the pump intensity is shown in Figure 5a. Devices with L ≥ 300 nm show a linear increase of the integrated Stokes intensity of the Ge TO peak for all investigated pump intensities, indicating that merely spontaneous Raman scattering occurs. In contrast, the integrated Stokes intensity of the Ge TO peak of devices with L = 20 nm, 50 nm and 100 nm, became nonlinear for sufficiently high pump intensities, suggesting the onset of SRS. Considering the smallest 20 nm long Ge nanodisc heterostructure device at a pump intensity of 60 kW/cm², the integrated

Stokes intensity of the Ge TO peak was twice the value calculated from linear extrapolation at the lowest pump intensities, corresponding to a 100% enhancement in Stokes scattering. A comparison of the integrated Ge TO signal to the substrate related Si TO and SiO_2 signals is shown in Figure S5.

Figure 5b shows the evaluation of the normalized integrated Stokes intensity of the Ge TO peak at a pump intensity of 256 kW/cm² as a function of the Ge segment length. The rapid increase in electric energy for Ge segment lengths < 100 nm, indicates a nanocavity effect within the Al-Ge-Al NW heterostructure device geometry.

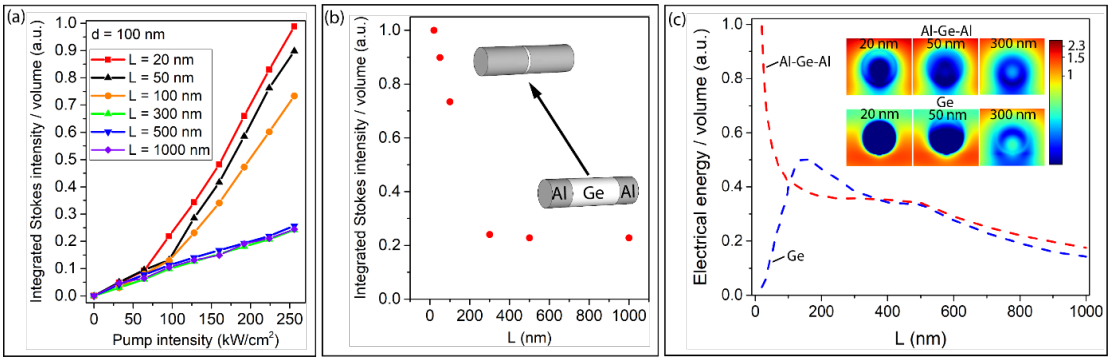

Figure 5. *(a) Temperature corrected integrated Stokes intensity of the Ge TO peak for Al-Ge-Al NW heterostructures as a function of the pump intensity normalized with respect to the volume of the Ge segment. Ge segment lengths vary between 20 nm and 1µm. The solid lines are a guidance for the eye. (b) Evaluation of the normalized integrated Stokes intensity of the Ge TO peak at 256 kW/cm² pump intensity as a function of the Ge segment length L. The inset is schematically showing the transition from heterostructure devices with Ge segments to Ge nanodiscs. All µ-Raman measurements were obtained using a λ = 532 nm pump laser. (c) Calculated electric field energy for bare Ge NWs (blue) and Al-Ge-Al NW heterostructures (red) normalized by both Ge volume and the effect of relative heating. The temperature corrections for (c) are shown in the supporting information (cf. Figure S6). The inset shows*

cross-sections of the field intensity distributions ($\left|E_p(\boldsymbol{r})\right|^2/|E_0|^2$) in the Ge segments for L= 20 nm, 50 nm and 300 nm.

The spontaneous Raman signal strength, S_R, depends on the electric field energy, $\frac{n^2}{2}\int_{V_{Ge}}\left|E_p(\boldsymbol{r})\right|^2 dV$, within the Ge volume, V_{Ge}, where $E_p(\boldsymbol{r})$ is the incident electric field. It will also be affected by the temperature, which can be taken into account by a correction function determined from the experiments, $f(L)$. We thus can write the normalized Raman signal per unit volume as $S_{R,n} \propto W_{CE} = \frac{f(L)}{V_{Ge}}\int_{V_{Ge}}\left|E_p(\boldsymbol{r})\right|^2 dV$, where W_{CE} has units of electric energy density. Calculations of W_{CE} are depicted for the bare Ge NW as well as the Al-Ge-Al heterostructure in Figure 5c. The correction data $f(L)$ and the non-corrected calculations are also shown for comparison in Figure S6. Most notably, the electric energy density increases for L < 100 nm in the Al-Ge-Al heterostructure (red dashed line), which indicates good optical confinement. This is in stark contrast to the Ge-only case, which shows a strong decrease for L < 100 nm (blue dashed line), indicating the loss of optical confinement. In fact, very little of the electric field penetrates the NW for segments of length, L < 100 nm as shown in the inset of Figure 5c. For the Al-Ge-Al heterostructure (inset Figure 5c, upper row), a hybrid plasmonic mode exists allowing for non-vanishing fields within the Ge even for the very shortest Ge-segments. Note that this is in line with results from Fan *et al*.[32] where a Ge NW resonance was cascaded with a metallic slit resonance formed between two narrow metal electrodes to support standing wave resonances of gap surface plasmon-polaritons.[33,34] These experimental observations and field calculations show that the metallic contacts are key to observing SRS within the narrow Ge-segment regime. The Al contacts to the Ge provide two functions: 1) optical confinement *via* a hybrid plasmonic mode to ensure a sufficiently large electric energy density to trigger SRS; and 2) the mitigation of Ge heating under the intense laser excitation.

CONCLUSION

In conclusion, we have systematically investigated Raman scattering in Ge NWs as well as axial Al-Ge-Al NW heterostructures with abrupt metal-semiconductor interfaces. We demonstrated that these quasi-1D heterostructures can be reassembled into Ge segments that are monolithically integrated between c-Al mirrors that also serve as effective heat-sinks. Plasmonic mode resonances within these nanocavities result in SRS with thresholds as low as 60 kW/cm^2. This is a significant step toward the development of a homogeneous group-IV nanolaser with low lasing threshold, which could lead to the development of the first monolithically integrable Ge based Raman nanolaser in the infrared as well as telecom wavelength range.

ASSOCIATED CONTENT

Supporting Information Available:

Laser induced heating effects of Ge NWs, TEM and EDX images of Al-Ge-Al NW heterostructures, details regarding the calculation of electric field energy for bare Ge NWs and Al-Ge-Al NW heterostructures with respect to the effect of heating. This material is available free of charge via the Internet at http://pubs.acs.org.

AUTHOR INFORMATION

Corresponding Author

*E-mail: alois.lugstein@tuwien.ac.at

Author Contributions

M.S. and M.G.B. performed the device fabrication. M.S. conducted the Raman measurements. A.L. conceived the project, contributed essentially to the experimental design. N.A.G. conducted the electric field energy calculations and the FDTD field intensity simulations for bare Ge NWs and Al-Ge-Al NW heterostructures. N.A.G. and R.F.O. assisted with the explanation of the underlying physical mechanisms. H.K. performed the numerical calculation of the spatial distribution of the electric field intensity *via* the FDTD method. M.I.H., E.R. and L.M.A. carried out the TEM and EDX measurements and analysis. All authors analyzed the results and helped shape the research and manuscript.

ACKNOWLEDGMENT

The authors gratefully acknowledge financial support by the Austrian Science Fund (FWF): project No. P29729-N27. The authors further thank the Center for Micro- and Nanostructures for providing the cleanroom facilities. We acknowledge support from the Laboratoire d'excellence LANEF in Grenoble (ANR-10-LABX-51-01). Financial support from the ANR-COSMOS (ANR-12-JS10-0002) project is acknowledged. We benefitted from the access to the Nano characterization platform (PFNC) in CEA Minatec Grenoble in collaboration with the LEMMA/IRIG group. We acknowledge support from Campus France in the framework of PHC AMADEUS 2016 for PROJET N° 35592PB.

REFERENCES

(1) Chau, R.; Doyle, B.; Datta, S.; Kavalieros, J.; Zhang, K. Integrated Nanoelectronics for the Future. *Nature Materials* **2007**, *6*, 810–812.

(2) Moore, G. E. Cramming More Components onto Integrated Circuits. *IEEE Solid-State Circuits Society Newsletter* **2006**, *11*, 33–35.

(3) Thompson, S. E.; Parthasarathy, S. Moore's Law: The Future of Si Microelectronics. *Materials Today* **2006**, *9*, 20–25.

(4) Chaudhry, A. Interconnects for Nanoscale MOSFET Technology: A Review. *Journal of Semiconductors* **2013**, *34*, 066001.

(5) Kaushik, B. K.; Goel, S.; Rauthan, G. Future VLSI Interconnects: Optical Fiber or Carbon Nanotube – a Review. *Microelectronics International* **2007**, *24*, 53–63.

(6) Soref, R. Silicon Photonics: A Review of Recent Literature. *Silicon* **2010**, *2*, 1–6.

(7) Wang, K. C. *High-Speed Circuits for Lightwave Communications*; Selected topics in electronics and systems; World Scientific, 1999.

(8) Claps, R.; Raghunathan, V.; Dimitropoulos, D.; Jalali, B. Influence of Nonlinear Absorption on Raman Amplification in Silicon Waveguides. *Optics Express* **2004**, *12*, 2774.

(9) Jalali, B.; Fathpour, S. Silicon Photonics. *Journal of Lightwave Technology, Vol. 24, Issue 12, pp. 4600-4615* **2006**, *24*, 4600–4615.

(10) Rong, H.; Jones, R.; Liu, A.; Cohen, O.; Hak, D.; Fang, A.; Paniccia, M. A Continuous-Wave Raman Silicon Laser. *Nature* **2005**, *433*, 725–728.

(11) Rong, H.; Xu, S.; Kuo, Y.-H.; Sih, V.; Cohen, O.; Raday, O.; Paniccia, M. Low-Threshold Continuous-Wave Raman Silicon Laser. *Nature Photonics* **2007**, *1*, 232–

237.

(12) Appenzeller, J.; Knoch, J.; Bjork, M. T.; Riel, H.; Schmid, H.; Riess, W. Toward Nanowire Electronics. *IEEE Transactions on Electron Devices* **2008**, *55*, 2827–2845.

(13) Pauzauskie, P. J.; Yang, P. Nanowire Photonics. *Materials Today* **2006**, *9*, 36–45.

(14) Jianye Li, Deli Wang, R. R. L. *Advances in III-V Semiconductor Nanowires and Nanodevices*; Bentham Science Publishers, 2011.

(15) Wei, H.; Pan, D.; Zhang, S.; Li, Z.; Li, Q.; Liu, N.; Wang, W.; Xu, H. Plasmon Waveguiding in Nanowires. *Chemical Reviews* **2018**, *118*, 2882–2926.

(16) Gradečak, S.; Qian, F.; Li, Y.; Park, H.-G.; Lieber, C. M. GaN Nanowire Lasers with Low Lasing Thresholds. *Applied Physics Letters* **2005**, *87*, 173111.

(17) Duan, X.; Huang, Y.; Agarwal, R.; Lieber, C. M. Single-Nanowire Electrically Driven Lasers. *Nature* **2003**, *421*, 241–245.

(18) Wu, J.; Gupta, A. K.; Gutierrez, H. R.; Eklund, P. C. Cavity-Enhanced Stimulated Raman Scattering from Short GaP Nanowires. *Nano Letters* **2009**, *9*, 3252–3257.

(19) Agarwal, D.; Ren, M.-L.; Berger, J. S.; Yoo, J.; Pan, A.; Agarwal, R. Nanocavity-Enhanced Giant Stimulated Raman Scattering in Si Nanowires in the Visible Light Region. *Nano Letters* **2019**, *19*, 1204–1209.

(20) Agarwal, D.; Yoo, J.; Pan, A.; Agarwal, R. Cavity Engineering of Photon–Phonon Interactions in Si Nanocavities. *Nano Letters* **2019**, *19*, 7950–7956.

(21) Wagner, R. S.; Ellis, W. C. Vapor-Liquid-Solid Mechanism of Single Crystal Growth. *Applied Physics Letters* **1964**, *4*, 89–90.

(22) Kral, S.; Zeiner, C.; Stöger-Pollach, M.; Bertagnolli, E.; den Hertog, M. I.; Lopez-Haro, M.; Robin, E.; El Hajraoui, K.; Lugstein, A. Abrupt Schottky Junctions in Al/Ge

Nanowire Heterostructures. *Nano Letters* **2015**, *15*, 4783–4787.

(23) El Hajraoui, K.; Luong, M. A.; Robin, E.; Brunbauer, F.; Zeiner, C.; Lugstein, A.; Gentile, P.; Rouvière, J.-L.; Den Hertog, M. In Situ Transmission Electron Microscopy Analysis of Aluminum–Germanium Nanowire Solid-State Reaction. *Nano Letters* **2019**, *19*, 2897–2904.

(24) Parker, J. H.; Feldman, D. W.; Ashkin, M. Raman Scattering by Silicon and Germanium. *Physical Review* **1967**, *155*, 712–714.

(25) Richter, H.; Wang, Z. P.; Ley, L. The One Phonon Raman Spectrum in Microcrystalline Silicon. *Solid State Communications* **1981**, *39*, 625–629.

(26) Borowicz, P.; Latek, M.; Rzodkiewicz, W.; Łaszcz, A.; Czerwinski, A.; Ratajczak, J. Deep-Ultraviolet Raman Investigation of Silicon Oxide: Thin Film on Silicon Substrate versus Bulk Material. *Advances in Natural Sciences: Nanoscience and Nanotechnology* **2012**, *3*, 045003.

(27) Lugstein, A.; Mijić, M.; Burchhart, T.; Zeiner, C.; Langegger, R.; Schneider, M.; Schmid, U.; Bertagnolli, E. In Situ Monitoring of Joule Heating Effects in Germanium Nanowires by μ-Raman Spectroscopy. *Nanotechnology* **2013**, *24*, 065701.

(28) Taflove, A.; Hagness, S. C. *Computational Electrodynamics : The Finite-Difference Time-Domain Method*; Artech House, 2005.

(29) Saltonstall, C. B.; Serrano, J.; Norris, P. M.; Hopkins, P. E.; Beechem, T. E. Single Element Raman Thermometry. *Review of Scientific Instruments* **2013**, *84*, 064903.

(30) Zardo, I.; Conesa-Boj, S.; Peiro, F.; Morante, J. R.; Arbiol, J.; Uccelli, E.; Abstreiter, G.; Fontcuberta i Morral, A. Raman Spectroscopy of Wurtzite and Zinc-Blende GaAs Nanowires: Polarization Dependence, Selection Rules, and Strain Effects. *Physical*

Review B **2009**, *80*, 245324.

(31) Wang, J.; Gudiksen, M. S.; Duan, X.; Cui, Y.; Lieber, C. M. Highly Polarized Photoluminescence and Photodetection from Single Indium Phosphide Nanowires. *Science* **2001**, *293*, 1455–1457.

(32) Fan, P.; Huang, K. C. Y.; Cao, L.; Brongersma, M. L. Redesigning Photodetector Electrodes as an Optical Antenna. *Nano Letters* **2013**, *13*, 392–396.

(33) Bozhevolnyi, S. I.; Søndergaard, T. General Properties of Slow-Plasmon Resonant Nanostructures: Nano-Antennas and Resonators. *Optics Express* **2007**, *15*, 10869.

(34) Chandran, A.; Barnard, E. S.; White, J. S.; Brongersma, M. L. Metal-Dielectric-Metal Surface Plasmon-Polariton Resonators. *Physical Review B* **2012**, *85*, 085416.

TOC GRAPHIC